Optimal Chine Nose Shape for Asymmetric Vortex Control at High Angle of Attack

M- Y. Park, H-U. Park*, S. H. Park*, J- W. Lee* and Y- H. Byun**
** Department of Aerospace Information Engineering Konkuk University*
1 Hwayang-dong, Gwangjin-gu, Seoul, 143-701, South Korea

Abstract
At the high angle of attack flight, flow separation is generated by free shear layer and a symmetry vortex flow having spiral point is created, but in case of above 30°, wake flow turns into turbulent, creating an asymmetric vortex. That induces lift reduction, unsought increased side force and yawing moment. Consequently, making the stability and controllability of flying vehicles get worse. However, lots of studies have been performed to overcome the stability reduction, caused by asymmetric rolled-up vortices at the high angle of attack and chine nose is suggested to lessen that reduction. Flying vehicles having chine shape reduce asymmetric flow at the high angle of attack and has more stability than general slender body-shaped flying ones.
The purpose of this study is to analyze the aerodynamics characteristics of missiles at high angle of attack right after the launch, aerodynamic characteristics and stability of the chine nose shape. Chine nose configuration is expressed by NURBS curve. The objective function is maximizing the lift to drag ratio (*L/D*) and $C_{n\beta}$, Yawing moment due to sideslip. The design constraint is *L/D*. The *L/D* must be larger than baseline. The repetitive response surface enhancement technique (RRSET) is proposed as a new system approximation method for the efficient optimum design.

1. Introduction

After appearance of long range air to air missiles, importance of BVR(Beyond Visual Range) engagement capability is increasing in air warfare. Such long range missile was efficient to only low maneuverability target in the early days but today, it is required capability of pursuit a high maneuverability target like new generation fighters. Even when missile is in high maneuver situation with high angle of attack, nevertheless it must have the capability of target tracking in those situations.
The feature of flow characteristic surrounding an elongated slender body is generally categorized according to the angle of attack. At a low angle of attack range of less than 15° ($0° \leq \alpha \leq 15°$), flow represents attached, symmetric and steady flow patterns. At middle angle of attack ($15° \leq \alpha \leq 30°$), two symmetric rolled-up vortices are generated and therefore the lift of the angle of attack increases non-linearly and pattern of flow is separated flow. Flow at a high angle of attack ($30° \leq \alpha \leq 60°$) is separated and steady/unsteady and asymmetric rolled-up vortices are formed. At greater than ($\alpha \leq 60°$), an unsteady turbulence wake is formed and post stall is created. The each angle of attack range can be changed by the shapes of the aircraft or free stream condition[1].
What causes asymmetric rolled-up vortex at more than high angle of attack is still unknown, but two representative theories for that question are the absolute instability theory and the convective instability theory. Many researchers have made an effort to discover the causes of asymmetric rolled-up vortices and their physical characteristics through both experimental and numerical studies. However, a flow field is formed by a very infinitesimal asymmetric disturbance, it is nearly impossible to interpret the field under perfectly symmetric conditions.
A number of studies have been performed to overcome the stability reduction caused by asymmetric rolled-up vortices at a high angle of attack in sub-sonic flow. Ravi and Mason, among others, have suggested a chine nose to lessen this reduction. Aircraft having chine shape experience reduced asymmetric flow at the high attack angle and have more stability than those with a more general slender body-shape. On the other hand, chine nose increase wetted area and cross section, so it induces decrease performance like that maximum speed or maximum range[2].
The purpose of this study is design a chine nose shape which maximizes direction stability at 40 degree angle of attack while satisfying the required drag and lift to drag ratio. RRSET[3,4](Repetitive Response Surface Enhancement Technique) and the global optimization technique are used for the derivation of the optimized solution.

2. Analysis method

2.1 Computational fluid analyses of chine shapes

In this study, CFD-FASTRAN[5] is used for the computational fluid analysis. The three-dimensional compressible Navier-Stoke equations are used as the governing equations and viscosity coefficient μ and Pr, the Prandtl number are separated into laminar flow part and turbulent one as below.

$$\mu = \mu_l + \mu_t$$
$$\frac{\mu}{\Pr} = \frac{\mu_l}{\Pr_l} + \frac{\mu_t}{\Pr_t} \quad \textbf{(1)}$$

Here, μ_l was used as a form of Sutherland law.

The governing equations are written as shown below when indicated as vector at orthogonal coordinates system of x, y, z.

$$\frac{\partial \vec{Q}}{\partial t} + \frac{\partial \vec{E}}{\partial x} + \frac{\partial \vec{F}}{\partial y} + \frac{\partial \vec{G}}{\partial z} = \frac{\partial \vec{E_v}}{\partial x} + \frac{\partial \vec{F_v}}{\partial y} + \frac{\partial \vec{G_v}}{\partial z} \quad \textbf{(2)}$$

$$\vec{Q} = \begin{bmatrix} \rho \\ \rho u \\ \rho \upsilon \\ \rho w \\ \rho e_t \end{bmatrix}, \vec{E} = \begin{bmatrix} \rho u \\ \rho u^2 + p \\ \rho u \upsilon \\ \rho u w \\ (\rho e_t + p) u \end{bmatrix}, \vec{F} = \begin{bmatrix} \rho \upsilon \\ \rho u \upsilon \\ \rho \upsilon^2 \\ \rho \upsilon w \\ (\rho e_t + p) \upsilon \end{bmatrix}, \vec{G} = \begin{bmatrix} \rho w \\ \rho u w \\ \rho \upsilon w \\ \rho w^2 + p \\ (\rho e_t + p) w \end{bmatrix} \quad \textbf{(3)}$$

$$\vec{E_\upsilon} = \frac{1}{Ra_\infty} \begin{bmatrix} 0 \\ \tau_{xx} \\ \tau_{xy} \\ \tau_{xz} \\ \beta_x \end{bmatrix}, \vec{F_v} = \frac{1}{Ra_\infty} \begin{bmatrix} 0 \\ \tau_{yx} \\ \tau_{yy} \\ \tau_{yz} \\ \beta_y \end{bmatrix}, \vec{G_v} = \frac{1}{Ra_\infty} \begin{bmatrix} 0 \\ \tau_{zx} \\ \tau_{zy} \\ \tau_{zz} \\ \beta_z \end{bmatrix} \quad \textbf{(4)}$$

where, Q is the conservative variable vector, ρ is the density of the air, p is the pressure, u, v and w are the velocity components, e_t is the total energy per unit mass.

We used Spalart-Allmaras one Equation turbulent model[6] for efficiency and convenience. Transformation equation is shown below.

$$\frac{d\bar{v}}{dt} = \left(\frac{1 + C_{b_2}}{\sigma} \right) \nabla \bullet [(v + \bar{v}) \nabla \bar{v}] - \frac{C_{b_2}}{\sigma} (v + \bar{v}) \nabla^2$$
$$+ C_{b_2} (1 - f_{t_2}) \overline{vS} - \left[C_{w1} f_w - \frac{C_{b_1}}{k^2} f_{t_2} \right] \left[\frac{\bar{v}}{d} \right]^2 + f_{t_1} (\nabla q)^2 \quad \textbf{(5)}$$

Roe's Flux Difference Splitting (FDS)[7] scheme is used for the spatial discretization with the Monotonic Upstream-Centered Scheme for Conservation Laws (MUSCL)[8] for higher order extension. The minmod limiter[8] is used to remove solution oscillation. The fully implicit Point Jacobi scheme is used for the time integration scheme[9].

The cross section shapes are defined from the shapes of super-ellipse equation and NURBS curve. The dimensions of fuselage is like below ;

Length of fuselage : 8d (8 times of diameter)

Curved nose : 3d

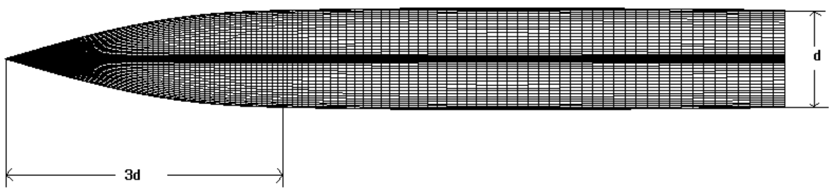

Figure 1. The grid shape of missile forebody

The free stream Mach number and the Reynolds number based on diameter are 2.0 and 6.9 x 10^5, respectively. The angle of attack and sideslip angle are 40 degree and 5 degree.

3. Trade study of chine shape

3.1 Super-ellipse equation

Ravi and Mason are using Super-ellipse equation to generate the cross section of chine shape. This equation is like below[10] :

$$\left(\frac{z}{b}\right)^{2+n} + \left(\frac{y}{a}\right)^{2+m} = 1, \quad \text{x} = \text{constant} \tag{6}$$

where n and m control the surface slopes at the top and bottom plane of symmetry and chine leading edge. The case $n = m = 0$ corresponds to the standard ellipse and the body is circular when $a = b$. In this study, the parameters n and m are taken to be constraints with respect to x. The parameters a and b are function of the axial location x, and can be varied to study planform effects. Notice that when $n = -1$, the value of m can be used to control the slope of the sidewall at the crease line[10].

3.2 Chine shapes generation

The super-ellipse equation is used for develop the various chine shape cross section. It is decided to analyze the effect of changing b/a, n and combinations thereof. Initially it is decided that the geometric parameters would be m = 0, and n would vary between -1 and -1.5. The value of b/a is varied between 0.5 and 1.5[10].
Using these design variables and equations, the chine shapes are generated by MATLAB to evaluate the results of reference 10 and aerodynamic characteristics analysis code. From design of experiment method, the 8 cases for test are derived. The table 4 shows the cases of super-ellipse equation.

Table 4. Super-ellipse Equation Case

	m	n	a	b
Case 1	0	-1.25	1	0.5
Case 2	0	-1.25	1	1
Case 3	0	-1.5	1	0.5
Case 4	0	-1.5	1	1
Case 5	1	-1.25	1	0.5
Case 6	1	-1.25	1	1
Case 7	1	-1.5	1	1

The chine shapes below are generated by design cases from DOE. The height of each cross section is same when using computational fluid dynamics.

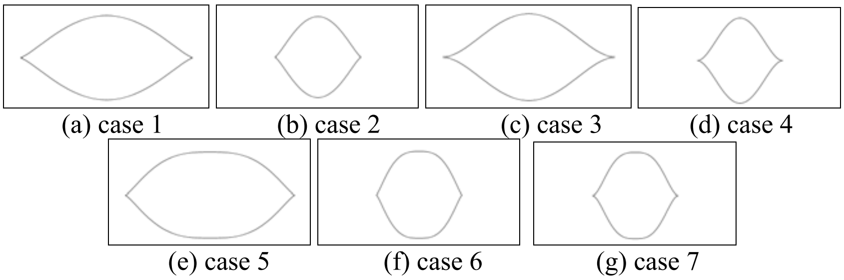

(a) case 1 (b) case 2 (c) case 3 (d) case 4
(e) case 5 (f) case 6 (g) case 7

Figure 2. Chine shapes are generated by super ellipse equation

3.3 Results of computational fluid analysis

To simulate the asymmetry vortex by CFD analysis, the side slip angle is given for 5°. Figure 8 (a) shows the density distribution of the flow over the missile cross section at the location of x/L = 0.8, and (b) shows the vector field of U direction at the same location of (a). From these figures, asymmetry vortex from side slip angle and bow shock from the blunt body is detected.

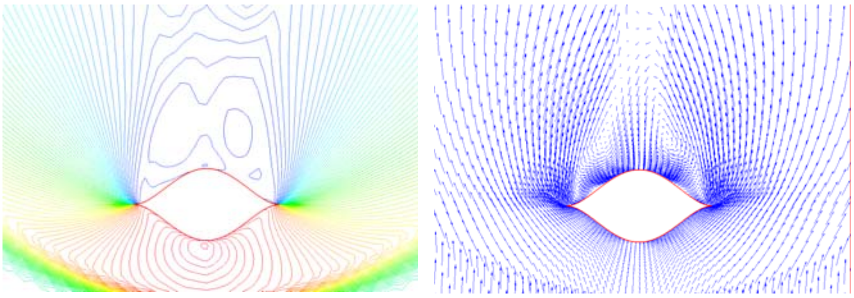

(a) Density distribution (b) Vector field

Figure 3. CFD results of case 3 at the x/L = 0.8 (AOA=20°)

Figure 9 is showing the side force coefficients, L/D and overall measure value.

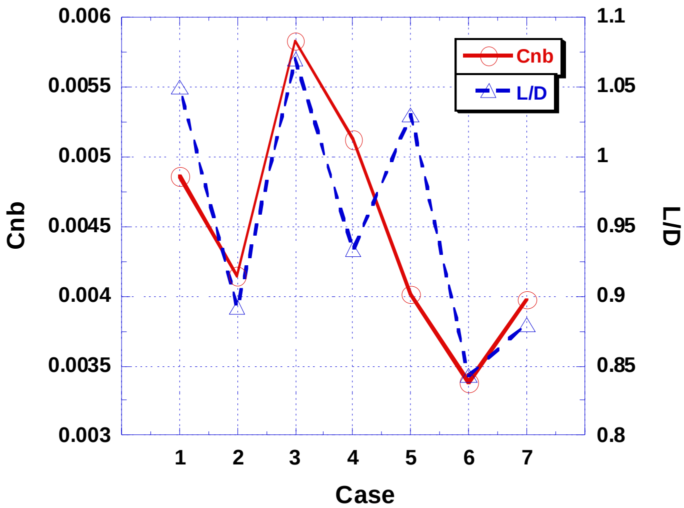

Figure 4. Yawing moment coefficient and L/D of each case

4 . Optimization of the chine shapes from NURBS curve

4.1 NURBS curve

NURBS(Non-Uniform Rational B-Splines) are a configuration modelling technique for drawing curves. NURBS curve are defined by a set of weighted control points, the order of curve and a knot vector. The knot vector is a sequence of parameter values that determine the continuity along the NURBS curve. The number of knots is always equal to the number of control points plus the order of the curve.

The order of the curve is greater or equal to 2, corresponding to a linear curve (order = 2), a quadratic curve (order = 3) and a cubic curve (order = 4). The curve is represented mathematically by a polynomial of same order; a cubic curve is represented by a degree 3 polynomial which order is 4. Besides, the number of control points must be equal to or greater than the order of the curve.

However, one of the drawbacks NURBS have, is the need for extra storage to define traditional shapes (e.g. circles). This results from parameters in addition to the control points, but finally allows the desired flexibility for defining parametric shapes. NURBS-shapes are not only defined by control points; weights, associated with each control point are also necessary. A NURBS curve $C(u)$, for examples, which is a vector-valued piecewise rational polynomial function, is defined as:

$$C(u)=\frac{\sum_{i=0}^{n} N_{i,k}(u)\cdot w_i \cdot p_i}{\sum_{i=0}^{n} N_{i,k}(u)\cdot w_i} \quad , \qquad 0 \le u \le n\text{-}k+2 \tag{7}$$

where w_i : Weights

p_i : Control points (vector)

$N_{i,k}(u)$: Normalized B-spline basis functions of degree k

t_i : knots forming a knot vector.

These B-splines are defined recursively as:

$$\begin{aligned}
&\boldsymbol{N_{i,k}(u)=\frac{(u-t_i)N_{i,k-1}(u)}{t_{i+k-1}-t_i}+\frac{(t_{i+k}-u)N_{i+1,k-1}(u)}{t_{i+k}-t_{i+1}}}\\
&\boldsymbol{N_{i,1}(u)=\begin{cases}1\leftarrow(t_i\le u\le t_{i+1})\\ 0\leftarrow(otherwise)\end{cases},\quad t_i\begin{cases}0\leftarrow(0\le i\le k)\\ i-k+1\leftarrow(k\le i\le n)\\ n-k+2\leftarrow(n<i\le n+k)\end{cases}}
\end{aligned} \tag{8}$$

4.2 Shapes generated from NURBS curve

Several of control points should be considered to generate the NURBS curve. When employing many control points, these are occurred unnecessary wave configuration. On the other hands, the chine shape generation is very difficult with small number of control point. Through several experiment, six control point have been selected reduce the computing time.

To decrease the design case, the design points of NURBS curve are selected. The three design variables of six control points are varies in rage of each point and others are fixed. Total 18 experiment points are selected to derive approximation model for optimization problem. Table 5 shows the control points to generate the chine shapes. The chine shapes are based on the case 3 of Fig. 3. Y and Z coordinates of control point two and Z coordinate of control point three are selected to configuration generate for this study.

Table 5. NURBS Curve Control Point

point no.	Y			Z		
	Min		Max	Min		max
1		0 (fixed)			0 (fixed)	
2	0	0.1	0.2	0		0.05
3		0.4 (fixed)		0.05	0.1	0.175
4		0.6 (fixed)			0.325 (fixed)	
5		0.9 (fixed)			0.5 (fixed)	
6		1 (fixed)			0.5 (fixed)	

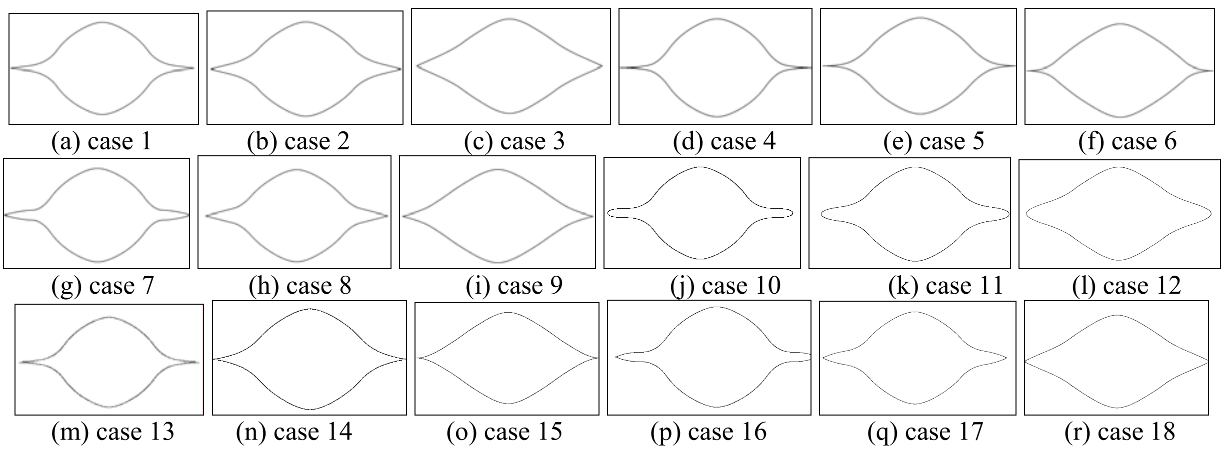

Figure 5. Chine shapes are generated by NURBS curve

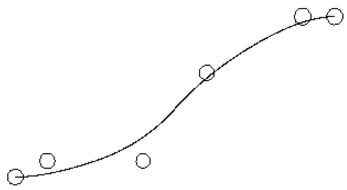

Figure 6. Control points of NURBS curve for chine shapes

4.3 Optimization problem formulation

The optimization problem formulation is given at table 1.

Table 1. Optimization problem formulation

Objective function	OMV (given at eqn. 6)	
Design Variables	Control points of NURBS curve	
	X1	Y coordinate of control point 2
	X2	Z coordinate of control point 2
	X3	Z coordinate of control point 3
Constraints	1.065(*L/D* of baseline) < *L/D*	

OMV (Overall Measure Value) is used for treat two objects at once. In this study, the objective function to maximize lift to drag ratio (*L/D*) and $C_{n\beta}$, yawing moment due to sideslip (angle of attack: 40 deg., sideslip: 5 deg.). A weighting factor $\omega=0.5$ is applied to consider different design conditions.

$$OMV = w \times \frac{C_{n\beta}}{(C_{n\beta})_{Baseline}} + (1-w) \times \frac{(L/D)}{(L/D)_{Baseline}} \tag{9}$$

The design constraints are the lift to drag ratio(*L/D*) at M=2.5 and angle of attack=40 deg. The lift to drag ratio must be bigger than 1.065 (*L/D* of baseline).

4.4 Results of computational fluid analysis

These cases are analyzed by CFD FASTRAN using the same boundary condition and grid system with previous section. Figure 7 shows the pressure distribution and flow path of the case 4 that generated by NURBS curve. From this figure, high pressure contour at bottom surface of fore body and low pressure contour at upper surface are detected when the flow speed is M_∞=2.5.

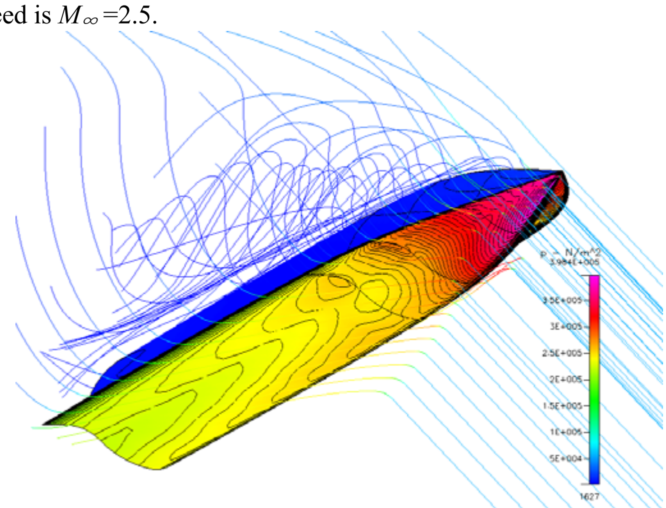

Figure 7. Pressure distribution and flow path of case 4 of NURBS curve

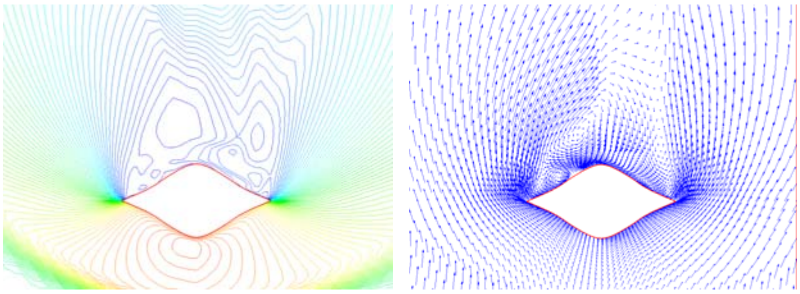

(a) Density distribution (b) Vector field

Figure 8. CFD results of case 4 at the x/L = 0.8 (AOA=40°)

Figure 8 shows the density contour and vector field of case 4 which generated by NURBS curve. When compare all results of these analysis, location and size of the secondary vortex are different because of the difference of the chine shapes.

The results of CFD analysis are compared in figure 9 by yawing moment coefficient and *L/D*. From these results, the case 4 is the best configuration for stability. On the other hand, the case 3 has worst results.

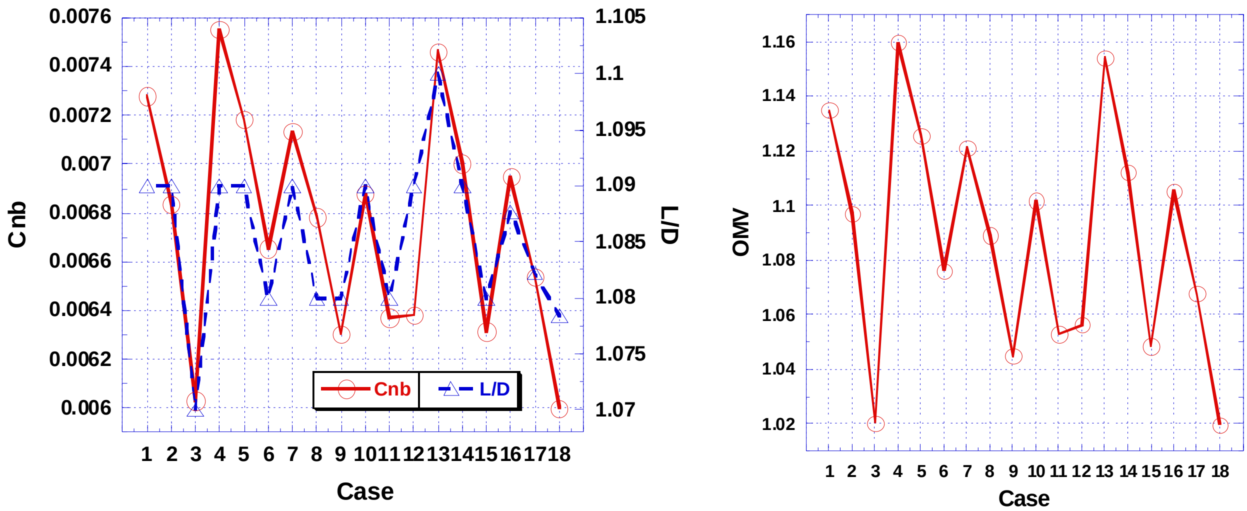

Figure 9. Yawing moment coefficient, L/D and OMV of each NURBS case

4.5 Chine Shape Optimization

According to design of experiments, eighteen design points are selected for analysis. Using these results, RRSET[3,4] is applied to generate regression model for optimization. R_{adj}^2 of this regression model is 0.96 and it can be reliable.
In this study, GENOCOP III[11] is used for the derivation of the global optimized solution.

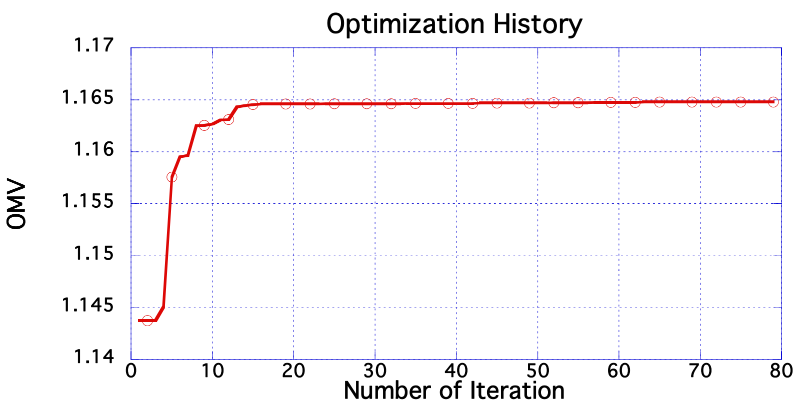

Figure 10. Optimization history from GENOCOP III

Table 2. Optimization Results

	Design Parameters	Baseline	Optimum Solution	Improvement Ratio
Design Variables	X1	0.1	0.0	
	X2	0.0	0.04361	
	X3	0.1	0.05	
Results	OMV(ω = 0.5)	1	1.1648	16.48%

5. Conclusions and future work

The shape optimization of the missile nose, which is currently emerging as an alternative for the stable operation of the latest aerial vehicle under a high angle of attack, is performed. The case study of chine shape is performed using super ellipse equation to verify the analysis tool and select the best configuration. The chine shapes are generated by NUBRS curve to derive an approximation model. Missile nose shape is optimized and its characteristic of high angle of attack is improved than circular and baseline configuration. The optimized shape from this research has shape edge of chine so, it generate strong vortex and it gives directional stability

6. Acknowledgments

The study was supported by the Brain Korea-21 Program (BK21) and the Korea Research Foundation under grant number 2005-D00151.

References

[1] Rom J., High angle of attack aerodynamics, Springer-Verlag, 1992.
[2] Van Dyke M. An album of fluid motion, Stanford: The Parabolic Press, 1982.
[3] Lee J-W., Jeon K-S., Byun Y-H., and Kim S-J., Optimal space launcher design using a refined response surface method, *FSKD 2005*, Changsha, China, 27 - 29 August 2005.
[4] Lee J-W., Jeon K-S., Byun Y-H., Repetitive response surface enhancement technique through design space transformation and sub-optimization, *ICAS 2006 25th Congress of International Council of the Aeronautical Sciences*, Hamburg, Germany, 3 ~ 8 September 2006.
[5] CFD Research Corporation, 2004, CFD-FASTRAN Users Manual.
[6] Spalrt, P. and Allmars, S. A one-equation turbulence model for aerodynamic flows, *AIAA Paper*, 92-0439, 1992
[7] Roe, P. L., Approximation Riemann solvers, parameter vectors, and difference schemes, *Journal of Computational Physics,* Vol. 43 pp.357-372, 1981
[8] Hirsch, C., Second-order upwind and high-resolution schemes, Numerical Computation of Internal and External Flows Vol. 2, John Wiley & Sons, New Jerjey, 1988, pp. 493-594.
[9] Pindera, M.Z, Yang, H.Q., Przekwas and Tucker, K., Assessment of modern method of numerical simulations of high speed flows", *AIAA Paper*, 93-0052, 1993.
[10] R. Ravi and William H. Mason, Chine shaped forebody effects on directional stability at high-α, *Journal of Aircraft*, Vol. 31, No. 3, May-June, 1994.
[11] Rao, S. S., Engineering Optimization, John Wiley and Sons, 1996, New York, USA

This page has been purposedly left blank